Modelling the artificial forest (*Robinia pseudoacacia* L.) root-soil water interactions in the Loess Plateau, China

Hongyu Li[1,2], Yi Luo[1,2,3], Lin Sun[1], Xiangdong Li[4], Changkun Ma[5], Xiaolei Wang[1,2], Ting Jiang[1,2], Haoyang Zhu[1,2]

[1] Key Laboratory of Ecosystem Network Observation and Modeling, Institute of Geographic Sciences and Natural Resources Research, Chinese Academy of Sciences, Beijing, 100101, China
[2] University of Chinese Academy of Sciences, Beijing, 100049, China
[3] Research Centre for Ecology and Environment of Central Asia, Chinese Academy of Sciences, Urumqi, 830011, China
[4] Guangdong Key Laboratory of Integrated Agro-environmental Pollution Control and Management, Guangdong Institute of Eco-environmental Science & Technology, Guangzhou, 510650, China
[5] State Key Laboratory of Eco-hydraulics in Northwest Arid Region, Xi'an University of Technology, Xi'an, 710048, China

Correspondence to: Yi Luo (luoyi@igsnrr.ac.cn)

Abstract. Plant root–soil water interactions are fundamental to vegetation–water relationships. Soil water availability and distribution impact the temporal–spatial dynamics of roots and vice versa. In the Loess Plateau (LP) of China, where semiarid and arid climates and deep loess soil predominant, drying soil layers (DSLs) have been extensively reported in artificial forestland. However, the underlying mechanisms remain unclear, but hypothetically involved root-soil water interactions. Although available root growth models are weak in simulating the rooting depth, this study addresses the hypothesis using a root growth model that simulates both the dynamic rooting depth and fine root distribution, coupled with soil water, based on cost–benefit optimisation. Evaluation of field data from an artificial forest site of black locust (*Robinia pseudoacacia* L.) in the southern LP positively proves its performance. Further, a long-term simulation, forced by a 50-year climatic data series with varying precipitation, was performed to examine the DSLs. The results demonstrate that incorporating the dynamic rooting depth into the current root growth models is necessary for reproducing soil drying processes. The simulations revealed that the upper boundary of the DSLs fluctuates strongly with infiltration events, while the lower boundary extended successively with increasing rooting depth. Most infiltration was intercepted of most infiltration by the top 2.0 m layer, which was the most active zone of infiltration and root water uptake. Below this, the percentages of fine roots (5.0%) and water uptake (6.2%) were small but caused a persistently negative water balance and consequent DSLs. Therefore, the proposed root–water interaction approach succeeded in revealing the intrinsic properties of DSLs; their persistent extension and a lack of opportunities for recovery from the drying state may adversely affect the implementation of artificial afforestation in this region, as well as in other regions with similar climates and soils.

Key words: Root–soil water interaction; Root growth model; Cost–benefit optimisation; Drying soil layer; Loess Plateau

1 Introduction

Plant roots are a significant pathway of the soil–plant–atmosphere continuum (SPAC), which connects the aboveground parts of the plant and the soil environment (Feddes et al., 2001; Mencuccini et al., 2019) by extracting water from the soil to meet the evaporation demand of the canopy. This soil water uptake process is regulated by root profile properties, which are highly dynamic in response to variable soil water conditions (Schenk and Jackson, 2002; Fan et al., 2017). In particular, forest root structures are rather complex (e.g., have woody coarse roots for anchoring and non-woody fine roots for absorption), which enable diverse water exploration strategies for adaptation to changing environments (Mulia and Dupraz, 2006; Ivanov et al., 2012; Sivandran and Bras, 2013; Brunner et al., 2015). For example, in order to increase water uptake, forests tend to grow more roots in the wetter soil layers (i.e., root hydrotropism) or develop deep roots to extract deeper water resources (including deep soil water and groundwater) (Maeght et al., 2013; Bardgett et al., 2014; Phillips et al., 2016). The investigation also indicated that forest stands develop a complicated morphological distribution of roots and diverse root water uptake strategies to adapt to the diverse soil water status (Germon et al., 2020; Knighton et al., 2020). Therefore, plant root–soil water interaction is a key issue for understanding the forest–water relationship, which is inevitably an important part of ecohydrological models, fundamentally for plant water uptake (Smithwick et al., 2014).

Plant water uptake is usually taken as a sink term in water movement equations (Feddes et al., 2001; Clark et al., 2015). The sink term is expressed as a function of the morphological and hydrological traits of the roots and soils. Morphologically, the root profile contains two primary features, rooting depth and vertical distribution (Warren et al., 2015), which are commonly included in most current root uptake models. These features are usually considered static in most of the available hydrologic and terrestrial biospheric models (Luo et al., 2003; Warren et al., 2015). The maximum rooting depths are generally assumed to be static values which may differ from the plant functional types (Ostle et al., 2009). Meanwhile, the vertical root distribution is represented as an empirical function of root length density to soil depth over the root domain (Jackson et al., 1996; Zuo et al., 2004; Sivandran and Bras, 2012), which describes the morphological features of roots statically. These simplifications of the root features allow ease in practical applications to simulate the root uptake process. However, it is increasingly recognised that efforts should be made to account for root dynamics, especially when the coupling effects between plant growth and water availability are considered (Warren et al., 2015).

The dynamic roots indicate that the hydrologic or terrestrial biospheric models simulate growing roots under changing environmental conditions, for example, soil water status. This is further incorporated into the root water uptake models. In these process models, the dynamic root profiles may be accounted for by either the changing rooting depth (Gayler et al., 2014; Hashemian et al., 2015; Christina et al., 2017; Liu et al., 2020) or root density distribution (Schymanski et al., 2008; Wang et al., 2016; Wang et al., 2018a; Drewniak, 2019; Niu et al., 2020), which is not sufficient to describe the dynamic root adaptation to changing environmental conditions (Rudd et al., 2014). The rooting depth, root density distribution, soil water quantity, and its spatial distribution are interrelated, and their coupling should be reflected in the root water uptake modelling (Warren et al., 2015). Sakschewski et al. (2021) reviewed the root growth approaches in the current Earth system

models and concluded that "none of those studies have acknowledged resource investment, timing and physical constraints of tree rooting depth within a competitive environment". Therefore, they implemented variable rooting strategies and dynamic root growth into the LPJmL4.0 model. Their results indicated that "variable tree rooting strategies are key for modelling the distribution, productivity and evapotranspiration of tropical evergreen forests" in the tropical South America. In their model, the maximum rooting depth is estimated by the tree height through a logistic growth function and the vertical distribution of the fine roots follows a shape function. Notably, the interactions between plant roots and soil water were not considered.

To meet the water requirement, plants tend to develop more roots in water-rich zones (Germon et al., 2020). Within the root system, soil water is conveyed up to the aboveground parts through fine roots (<2 mm in diameter) and coarse roots (>2 mm diameter), the former for water uptake and the latter for water transport (Jackson et al., 1997; Smithwick et al., 2014). Fine roots are developed on coarse roots, together constituting a hydraulic architecture, creating structural relationships for water transport (Smithwick et al., 2014; Chen et al., 2019). According to the pipe model theory (Lehnebach et al., 2018), for denser fine roots to uptake more soil water, coarser roots are required to maintain the hydraulic transport capacity, especially for deeper extension. Balancing the cost of biomass allocation to coarse or fine roots and the benefit of the water taken up is a great ability of plants which live under water-stressed conditions (Guswa, 2008). Mathematical optimisation methods have been widely implemented in previous studies to estimate the optimal root profiles (Kleidon and Heimann, 1998; Collins and Bras, 2007; Guswa, 2008; Schymanski et al., 2008 and 2009; Yang et al., 2016). Nonetheless, optimisation efforts for root dynamic processes remain limited. The coupled effects of root growth and soil water should be the fundamentals to the optimization approach. An optimisation method will be surely beneficial for simultaneously estimating the dynamics of rooting depth and fine root distribution.

The drying soil layer is defined as a soil layer with soil water content between stable field capacity and permanent wilting point (Wang et al., 2011). This is a phenomenon of concerned and have been widely studied in the Loess Plateau of Northwest China. Huang and Shao (2019) reviewed the studies on drying soil layers in the Loess Plateau over the past decades, which indicated that the drying soil layers prevail in the artificial forestlands in the region and develop as the stand ages. It is generally believed that the drying soil layers are caused by limited rainfall infiltration and improper afforestation; however, the underlying mechanisms remain unclear and require exploration (Shao et al., 2018). Although rainfall is insufficient in the semi- and arid climates in the Loess Plateau, the thick loess soils store significant quantities of water for potential plant use. When water stress occurs in the upper soil layer due to insufficient infiltration, high atmospheric demand due to the aridity may cause plants to develop roots for using deeper soil water (Pierret et al., 2016). Thus, root–water interactions may play a key role in the occurrence and development of drying soil layers.

Many *in situ* investigations have reported that the drying soil layer has developed extensively in forests of black locust (*Robinia pseudoacacia* L.), which is the most popular and deep-rooted afforestation species in Loess Plateau (Deng et al., 2016; Jia et al., 2017b; Liang et al., 2018; Wu et al., 2021). Thus, the occurrence and evolution of the drying soil layer in this

forestland are worthy of discussion. Therefore, this study aimed to (1) develop a coupled soil water-root growth model based on the cost–benefit theory, which can simultaneously adjust root distribution and rooting depth in the root water uptake model, and (2) reveal the black locust root–soil water interactions throughout the soil profile, based on a long-term simulation, to address the drying soil layer issues in this region.

105   **2 Materials and methods**

2.1 Model development

2.1.1 General description to the ecohydrological model

Fundamentally, this ecohydrological model is an integration of different components from the Soil and Water Assessment Tool (SWAT) (Neitsch et al., 2011; Arnold et al., 2012) and Community Land Model version 4.5 (CLM4.5) (Oleson et al.,
110   2013) (Fig 1). On this basis, root growth and root uptake modules were modified. Furthermore, an optimisation approach was introduced to simulate the coupled effects of root growth and soil water dynamics.
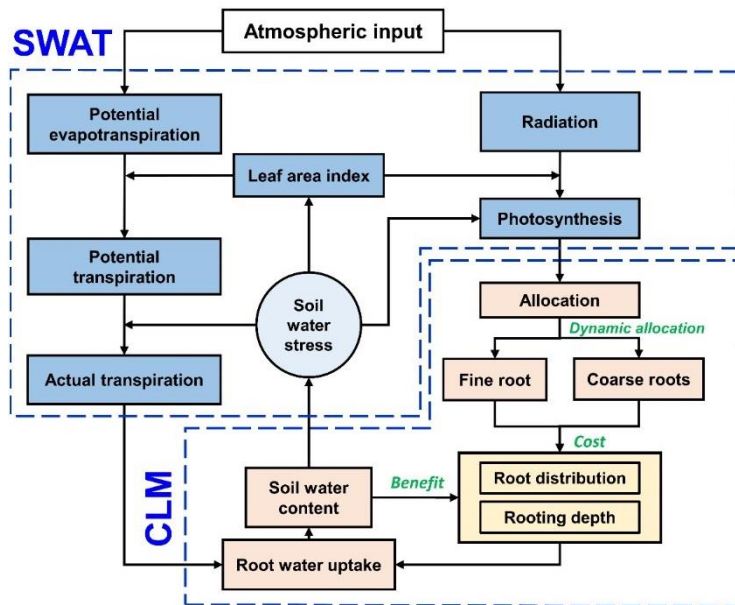
Figure 1: The model structure integrated from SWAT (blue boxes) and CLM (light orange boxes) components. The root growth module is highlighted in yellow, and the descriptions of the dynamic fine root distribution and rooting depth approach are
115   **illustrated as green text.**

Hydrologically, surface process modules, for example, simulating evaporation, transpiration, canopy interception, and runoff, follow the SWAT model which is detailed in its theoretical document (Neitsch et al., 2011). The subsurface

hydrological modules, primarily the soil water movement, adopted the 1-D Richards' equation. It is solved numerically
following the finite difference scheme used in CLM4.5 (Oleson et al., 2013).

Biologically, modules for the aboveground parts, for example, plant phenology, leaf area index (LAI) development, and biomass accumulation, are adopted from SWAT (Neitsch et al., 2011) and in CLM 4.5 (Oleson et al., 2013). The module for the belowground part, the root growth model, simulates root growth following CLM 4.5 which adopts the approaches from process simulation directly from the implementation in the Biome-BGC (Biome BioGeochemical Cycles) model (Thornton et al., 2002). See the **Supplementary File** for more information on the detailed model descriptions. In CLM 4.5, the roots are categorised into coarse and fine. The rooting depth is presented as a static value, and the fine root distribution follows a static shape function which defines the root density over the soil profile.

The root–water interaction is integrated into the root uptake model, which uses the rooting depth and fine root distribution as input and acts as a sink term in the Richards' equation. Soil water imposes water stress on the root growth. The cost of biomass invested in coarse and fine roots and the benefit of water uptake were optimised through a cost–benefit function.

The following sections will describe three root growth approaches in a stepwise manner: (1) the static root distribution approach implemented in CLM4.5, which assumes a static rooting depth of the coarse roots and distribution of fine roots (Oleson et al., 2013); (2) the approach that assumes a dynamic distribution of fine roots but a static rooting depth (Drewniak, 2019); and (3) the approach proposed in this study that assumes a dynamic distribution of fine roots and rooting depth of coarse roots. These three root growth modelling approaches are incorporated into the eco-hydrological model mentioned above for a comparison of their performances.

2.1.2 Static distributions of coarse and fine roots

In this approach, a static exponential function expresses the root fractions in different soil layers (Zeng, 2001):

$$
fr_i = \begin{cases} 0.5[\exp(-r_a z_{h,i-1}) + \exp(-r_b z_{h,i-1}) - & 1 \le i < n \\ \quad \exp(-r_a z_{h,i}) - \exp(-r_b z_{h,i})] & \\ & \\ 0.5[\exp(-r_a z_{h,i-1}) + \exp(-r_b z_{h,i-1})] & i = n \end{cases}
\tag{1}
$$

where i is the sequential number of soil layers, n is the total number of soil layers in the rooting zone, $z_{h,i}$ is the depth of soil layer i, r_a and r_b are two shape parameters. The shape parameters can be obtained by fitting to the observations for different plant types, set as 4.8 and 0.8 according to fine root samplings in this study (see Section 2.2.4), respectively (Oleson et al., 2013).

2.1.3 Dynamic distribution of fine roots

This approach assumes that newly assimilated biomass to the belowground parts is allocated to develop fine and coarse roots with a static ratio. In general, there is a linear relationship between the carbon mass and biomass (Niu et al., 2020). Therefore, the term "carbon" will be used in the following text to refer to the biomass of different plant components. Within the present rooting depth (static over the simulation period), the fine roots are distributed over the soil depth according to the soil water content. In each soil layer i, the fine root carbon increment is updated at each time step, as follows:

$$FR_{i,t} = FR_{i,t-1} + \Delta FR_{i,t} \tag{2}$$

where $FR_{i,t-1}$ (g m^{-2} d^{-1}) is the fine root carbon of soil layer i during the previous time step, $\Delta FR_{i,t}$ (g m^{-2} d^{-1}) is the newly allocated carbon to fine roots of soil layer i at time t, which is modified by soil water content:

$$\Delta FR_{i,t} = \Delta FR \cdot \frac{THK_i REW_i}{\sum_{i=1}^{n}(THK_i REW_i)} \tag{3}$$

where ΔFR is the newly assimilated carbon allocated to total fine roots (g m^{-2} d^{-1}), n is the total number of soil layers in the rooting zone, Thk_i is the soil layer thickness of soil layer i (cm), REW_i is the relatively effective soil water content (i.e., soil water availability) given by:

$$REW_i = \frac{\theta - \theta_{wp}}{\theta_{fc} - \theta_{wp}} \tag{4}$$

where θ is the soil water content (cm^3 cm^{-3}), and the subscripts wp and fc indicate the soil water content at the wilting point and field capacity, respectively.

The fine root fraction in each soil layer i is then calculated:

$$fr_i = \frac{FR_{i,t}}{\sum_{i=1}^{n} FR_{i,t}} \tag{5}$$

2.1.4 Dynamic distributions of coarse and fine roots

This approach assumes that both the rooting depth of coarse roots and the distribution of fine roots change with soil water. In formulating the growth of the coarse and fine roots, the newly allocated biomass/carbon for the belowground part is optimally allocated to the roots based on a cost–benefit function that will be described in detail.

(1) Carbon allocation between the coarse and fine roots

The cost is defined as the amount of carbon invested to grow coarse/fine roots. In constructing the coarse and fine root systems, the pipe model theory (PMT, Shinozaki, 1964) was adopted. Lehnebach et al. (2018) summarised "the essence of the PMT concept" as "*a unit amount of leaves is provided with a pipe whose thickness or cross-sectional area is constant. The pipe serves both as the vascular passage and as the mechanical support and runs from the leaves to the stem through all intervening strata.*" The relationship between the leaf and stem can be established quantitatively based on the PMT and can

be extended to the belowground parts of the plants (Chen et al., 2019). For roots, the relationships have been established in analogue form and validated against some databases (Carlson and Harrington, 1987; Richardson and Dohna, 2003).

175 Delineating the soil profile into adjacent soil layers which correspond to the numerical solution of the Richards' equation, the equations for modelling the root growth are also written regarding the discrete soil layers (Fig 2c).
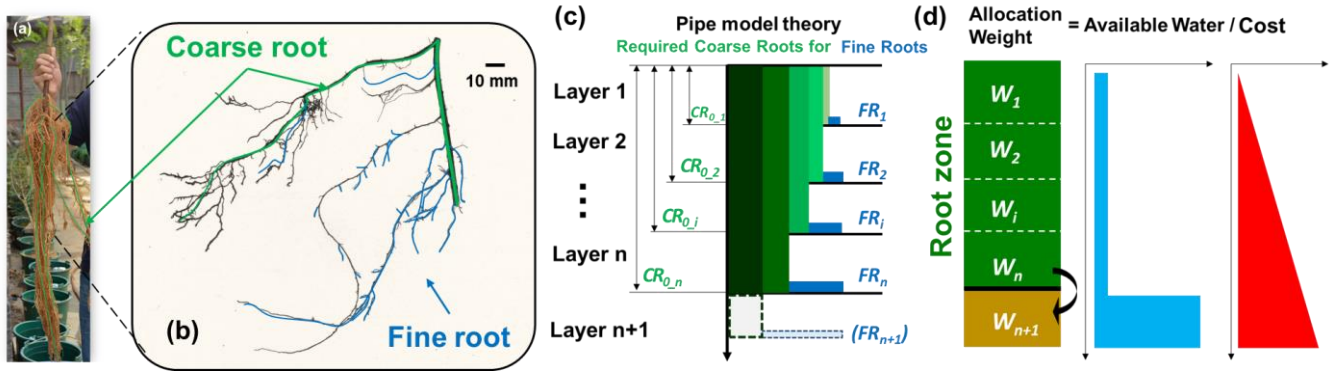
Figure 2: (a) Black locust root system obtained from an experimental pot; (b) scanned image of one root segment consisting of coarse and fine roots; (c) schematic description of pipe model theory adopted for coarse and fine roots; (d) weighting factors for
180 **carbon allocation and conceptualized benefit (available soil water for uptake) and cost (carbon investment)**

The carbon amount for coarse and fine roots should be maintained as

$$CR_{0\_i} = \rho \cdot Z_i \cdot k_A \cdot FR_i \tag{6}$$

where CR_{0_i} is the equivalent carbon for coarse roots in the zone between the ground surface and bottom of soil layer i, FR_i is the carbon for fine roots within the soil layer i, ρ is the mass density of coarse roots (g/cm^3), Z_i is the depth from
185 the surface to the bottom of soil layer i (cm), *and* k_A is a constant which can be determined from field observations (see Section 2.3.2).

For an increment of carbon for fine roots within soil layer i, a corresponding increment of carbon for coarse roots is needed and can be derived from Eqn. (6):

$$\Delta CR_{0\_i} = \rho \cdot Z_i \cdot k_A \cdot \Delta FR_i \tag{7}$$

190 Notably, there is no increment of carbon for coarse roots if the available coarse roots are sufficient to support the new fine roots, as discussed later.

The increments of carbon for fine and coarse roots were then summed over the root profile:

$$\Delta CR = \sum_1^n \Delta CR_{0\_i} \tag{8}$$

$$\Delta FR = \sum_1^n \Delta FR_i \tag{9}$$

195 The sum of the newly allocated carbon for fine and coarse roots is equal to that allocated to the belowground part ΔTR:

$$\Delta FR + \Delta CR = \Delta TR \tag{10}$$

Two ratios are defined for fine and coarse roots, respectively as:

$$K_{FR} = \frac{\Delta FR}{\Delta CR + \Delta FR}, \quad K_{CR} = \frac{\Delta CR}{\Delta CR + \Delta FR} \tag{11}$$

(2) Spatial distribution of new fine and coarse roots

Potentially, more fine roots develop in wetter soil zones to gain more water and reduce water stress to the least extent. It is fundamentally recognised that penetration into deeper soil requires carbon for the fine roots, as well as the corresponding coarse roots; the potential benefit can be more water uptake from the deeper soil. The basic principle for the distribution of the roots, either fine only or both coarse and fine, is that an optimal distribution of new roots helps to gain as much water as possible (Fig 2d).

Thus, the distribution of fine roots is influenced by a benefit-to-cost ratio, defined as:

$$W_i = \frac{REW_i}{CFR_i} \tag{12}$$

where W_i is the benefit to cost ratio in soil layer i, and the benefit is presented by REW_i, as defined previously; CFR_i is defined as the marginal carbon cost of fine roots:

$$CFR_i = \frac{\partial(\Delta CR_{0\_i} + \Delta FR_i)}{\partial \Delta FR_i} = \rho \cdot Z_i \cdot k_A + 1 \tag{13}$$

Combining Eq. (13) and Eq. (12):

$$W_i = \frac{REW_i}{\rho \cdot Z_i \cdot k_A + 1} \tag{14}$$

Replacing REW_i with W_i in Eq. (3), the fraction of new fine roots in the soil layer i becomes

$$\Delta FR_i = \Delta FR \cdot \frac{THK_i W_i}{\sum_{i=1}^{m}(THK_i W_i)} \tag{15}$$

Updating the fine root fractions using Eq. (7), the demand for coarse roots that can meet the hydraulic transport demand for the fine roots within and below soil layer i is

$$CRP_i = \sum_{j=i}^{n} CR_{0\_i,NEW} = \sum_{j=i}^{n} \rho \cdot Z_i \cdot k_A \cdot (FR_i + \Delta FR_i) \tag{16}$$

Comparing the demand for and current storage of coarse roots, the coefficient of the coarse root carbon increment regarding the soil layer i is calculated as

$$\beta_i = \frac{\max(CRP_i - CR_i, 0)}{\sum_{i=0}^{n} \max(CRP_i - CR_i, 0)} \tag{17}$$

According to Eq. (11), the increment of carbon for the coarse roots with respect to each soil layer is then calculated by:

$$\Delta CR_i = \Delta TR \cdot K_{CR} \cdot \beta_{ci} \tag{18}$$

(3) Rooting depth extending

To calculate the rooting depth extension via optimisation, the target function S_m is defined as follows:

$$S_m = \sum_{i=1}^{m}(thk_i \cdot fr_i \cdot REW_i) \tag{19}$$

When S_m reaches its maximum, the optimum distribution of new roots over the soil profile is obtained. If S_m reaches its maximum when m is equal to n, the length of the coarse root remains unchanged; when m is equal to $n + 1$, the coarse root penetrates the next soil layer.

2.2 Data

2.2.1 Site description

The study site is located in the Provincial Nature Forest Reserve, Yeheshan (34°31.76N, 107°54.67E; 1,090 m elevation), in the southern part of the Loess Plateau in China (Fig 3). The climate is semi-humid with an annual average temperature of 11.3 °C and precipitation of 570 mm (from Yongshou station, see 2.2.2). It is hot in summer and cold in winter, and precipitation occurs predominantly from May to October and varies significantly interannually. The artificially afforested black locust (*Robinia pseudoacacia* L.) dominates the vegetation species with an average height of 10 m (planted since 2000) and a density of 2,450 trees/ha² (Ma et al., 2017). The experimental plots were situated within a black locust forestland on an average slope of 8°. Instruments for the microclimate and soil water observations were installed. The thickness of the loess soil is estimated to be more than 50 m, and the buried depth of groundwater is beyond that depth (Liu et al., 2010).
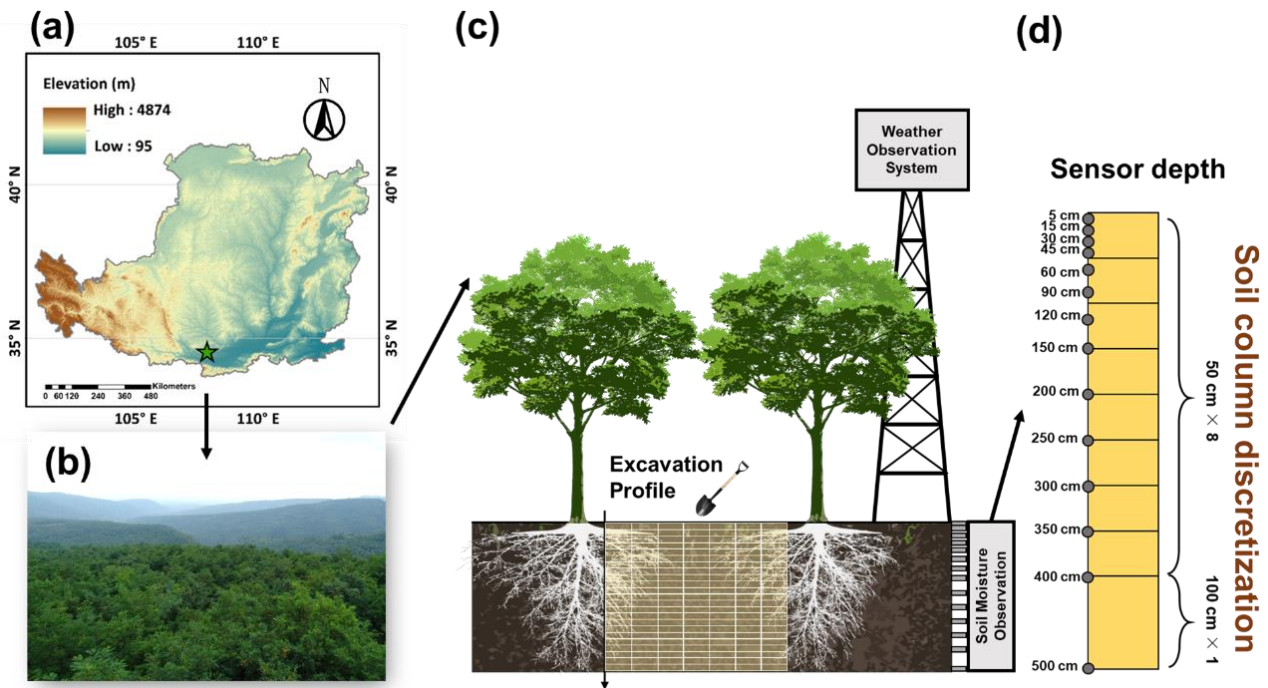
Figure 3: (a) Location of the study site in the Loess Plateau, China; (b) top view from the black locust plantation canopy in July, 2018; (c) meteorological observation tower, soil moisture observation, and excavation root profile; (d) installation of the soil moisture sensors.

2.2.2 Meteorology

A meteorological observation system was established on a flux tower in 2014. The tower was 16 m above the ground, higher than the tree canopy (Fig 3). This system consists of sensors for temperature and humidity, HMP155A probes (Campbell Scientific, Inc., Logan, UT, USA); for wind speed, the CSAT3 three-dimensional ultrasonic anemometer (Campbell Scientific, Inc., Logan, UT, USA); and for solar radiation, the CNR-4 net radiometer (Campbell Scientific, Inc., Logan, UT, USA). A T-200B precipitation gauge (Geonor Inc., Oslo, Norway) was installed near the forest opening to measure throughfall. A CR3000 data logger (Campbell Scientific, Inc., Logan, UT, USA) was used to collect data from the sensors at 10-min intervals.

In addition, daily meteorological data from 1971 to 2020 for the National Metrological Station in Yongshou County, 26 km away from the field experiment site, were downloaded from the China Meteorological Data Service Centre (http://data.cma.cn) for the long-term simulation. The data series include daily precipitation, mean air temperature, maximum air temperature, minimum air temperature, relative humidity, wind speed, and sunshine hours.

It is believed that the data series spanning 50 years covers the inter-annual variations in climatic factors, especially the alternating wet and dry periods (Fig 4). The annual average precipitation is 570 mm, with a standard deviation (STD) of 122 mm.
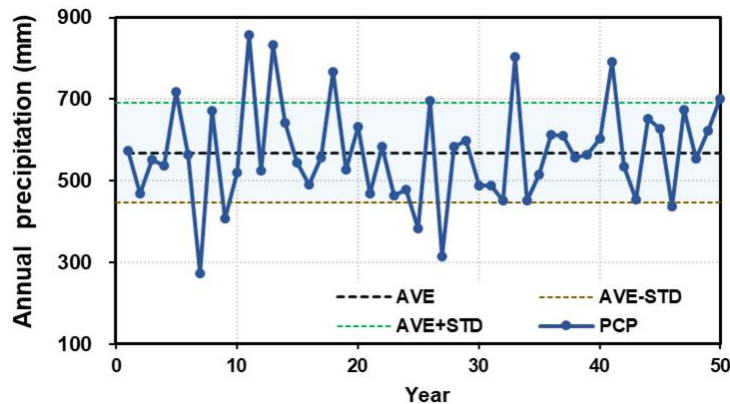
Figure 4: Time series of annual precipitation (mm). Dashed coloured lines represent the average values (AVE) and plus or minus one standard deviation (STD).

2.2.3 Soil and water

The soil properties were investigated by sampling over a profile 5.0 m below the ground at the study site. The dry bulk density (ρ_b, g cm^{-3}) was obtained by drying volumetric soil samples (100 cm^3) at 105 °C for 48 h, and the soil particle size distribution and organic matter content were measured in the laboratory. Silt loam dominated the profile, with moderate

265 variations among the soil layers. On average, the silt loam consisted of 5.8% sand, 73.4% silt, and 20.9% clay (Ma et al., 2017).

The saturated hydraulic conductivity (K_s, cm h^{-1}) was measured in the undisturbed soil samples using a constant-head method (Ramos et al., 2017). The field capacity (θ_{fc}) and wilting point (θ_{wp}) were derived from the power function (Campbell, 1974; Clapp and Hornberger, 1978), corresponding to the soil potentials of −33 kPa and −1,500 kPa,

270 respectively.

Volumetric soil moisture sensors were installed in 14 layers within the depth of 500 cm, at 5, 15, 30, 45, 60, 90, 120, 150, 200, 250, 300, 350, 400, and 500 cm, respectively (Fig 3). The sensors, CS-655 Soil Water Content Reflectometers (Campbell Scientific, Inc., Logan, UT, USA), have been in operation since June 2014. A CR1000 data logger (Campbell Scientific, Inc., Logan, UT, USA) records the data every 10 min.

275 The soil properties below 5.0 m were adopted from previous studies (Li et al., 2008; Jia et al., 2017a; Wu et al., 2021) on black locust plantations in the Loess Plateau.

The soil desiccation index (SDI) was used to evaluate the degree of soil desiccation for the comparison between the observation and simulation results, calculated as:

$$SDI = \frac{\theta - \theta_{wp}}{\theta_{sfc} - \theta_{wp}} \tag{20}$$

280 where θ_{sfc} is the soil water content at a stable field capacity. In practice, soil water content at 60% of field capacity (θ_{fc}) can be assumed to be the stable field capacity of loess in the Loess Plateau (Wang et al., 2011). Soil layers with SDI < 1 were regarded as the drying soil layers.

2.2.4 Plant

The leaf area index (LAI, m^2 m^{-2}) of the black locust canopy was measured using an optical method (Jonckheere et al.,

285 2004), biweekly or triweekly during the growing seasons of 2014, 2015, and 2016. An 8 mm fisheye lens (Sigma F3.5 EX DG Circular Fisheye-Sigma Corporation) mounted on a Canon EOS 5D digital SLR camera (http://www.canon.com) took hemispherical photographs of the canopy on cloudy days. The photographs were analysed using the CAN_EYE software to derive the LAI values (Demarez et al., 2008). Within each plot, photographs were taken at five different positions each time. The LAI value for the plot is the average of the five positions.

290 The measured LAI values were compared to those of the Moderate Resolution Imaging Spectroradiometer (MODIS) product MYD15A2H, which has a spatial resolution of 500 m and a temporal resolution of 8 d. Furthermore, the 8-d MODIS LAI series were downscaled to a daily series using the Savitzky–Golay filtering technique (Tie et al., 2017).

The root profiles were investigated in August 2015. A 150-cm wide trench was excavated 500 cm below the ground, which was located between two neighbouring rows, perpendicular to the row direction (Fig 3). During the excavation, soil

295 samples, 20 cm in horizontal dimensions and 40 cm in vertical thickness, were taken along the trench and over the profile. It

is assumed that the roots develop homogeneously along the horizontal row but unevenly along the trench. Finally, seven samples were collected from each soil layer across the trench. The soil samples were rinsed, and the weight and length of fine roots (less than 2 mm in diameter) were measured for each sample.

To estimate the parameters of the black locust root system, a pot experiment was carried out in 2016 (planted in April and sampled in October), the details of which are given in **Fig S1** in the **Supplementary File**.

In addition to the measurements mentioned above, data on black locust roots, including the density profile and rooting depth were compiled from the published literature (see **Supplementary File**).

2.3 Model setup

2.3.1 Initial and boundary conditions for the Richards' equation

In solving Richards' equation numerically, the vertical domain extends from the surface to 20 m below the ground. The domain was discretized into adjoining layers with a thickness of 5 cm each.

The upper boundary condition was set as the flux of the rainfall rate with the canopy interception removed or the soil evaporation rate. As the soil water content in deep soil (20-100 m) is relatively stable around the field capacity (Qiao et al., 2018), the lower boundary was set to a constant soil water content at the field capacity.

During the calibration and validation stages, the initial soil water profile was determined using the measurements. The initial soil water profile was set at the field capacity when the model was applied to the long-term simulation.

2.3.2 Numerical simulations

The soil hydraulic parameters, saturated hydraulic conductivity K_s and constant B in the soil water retention curve, were initialised by the measured values. They were further tuned to match the simulated soil water content to the observations.

The vegetation growth parameters were adapted from Zhang et al. (2015), who simulated the black locust growth in the Loess Plateau using the Biome-BGC model. Other vegetation parameters were obtained from the SWAT model (Neitsch et al., 2011; Sun et al., 2011).

All the relevant parameters are summarized in **Table S1**.

2.3.3 Numerical simulations

(1) The model calibration and validation were performed for the observation period (2014–2018). The model was calibrated from 1 June 2014 to 31 December 2016 and validated through 1 January 2017 to 31 December 2018. The measured LAI, soil water content, and root profiles were used for the evaluation. The rooting depth was assumed to be 5.0 m below the ground for three approaches, considering the relatively short period of the field experiment.

(2) A long-term simulation was performed to explore the forest root–soil water interactions over a period of 50 years, with the aim of investigating the drying soil layer evolution over the long term under inter-annual variations of precipitation.

The long-term simulation adopted the data at Yongshou Station from 1971 to 2020 without any sense of a specific historical period. In the long-term simulation, a value of 5.0 m was set for the rooting depth of the static approaches; an initial value of 50 cm was set for the dynamic rooting depth approach. Plants start to grow at the beginning of the simulation.

2.3.4 Evaluation indices

Statistical indices, the coefficient of determination (R^2), Nash-Sutcliffe efficiency (NSE), and percent bias ($PBIAS$), were used to evaluate model performance and are given as follows, respectively:

$$R^2 = \frac{\sum_{i=1}^{n}(S_i - \bar{S})(O_i - \bar{O})}{\sqrt{\sum_{i=1}^{n}(S_i - \bar{S})\sum_{i=1}^{n}(O_i - \bar{O})}} \tag{21}$$

$$NSE = 1 - \frac{\sum_{i=1}^{n}(O_i - S_i)^2}{\sum_{i=1}^{n}(O_i - \bar{O})^2} \tag{22}$$

$$PBIAS = \frac{\sum_{i=1}^{n}(S_i - O_i)}{\sum_{i=1}^{n} O_i} \times 100\% \tag{23}$$

where S_i is the simulated value at time step i, $\bar{S}$ is the mean of the simulated value, O_i is the observed value at time step i, $\bar{O}$ is the mean of the observed value, and n is the number of time steps. R^2 and NSE were dimensionless. The dimension of the $PBIAS$ was %.

R^2 describes the proportion of the variance in the measured data explained by the model, ranging from 0 to 1, with higher values indicating less error variance. NSE indicates the consistency between the plot of the observed versus simulated data and the 1:1 line, ranging between $-\infty$ and 1.0 (1 inclusive) and optimised at the value of 1. $PBIAS$ measures the average tendency of the simulated data to be larger or smaller than the observation, and a lower value implies a more accurate model simulation, with optimisation at 0.0. Positive values indicate a model underestimation bias, and negative values indicate a model overestimation bias. Moriasi et al. (2007) proposed a widely used rating system, which judged the modelling performance as "very good", "good", "satisfactory", or "unsatisfactory" using $PBIAS < \pm10\%$, $\pm10\% \leqslant PBIAS < \pm15\%$, $\pm15\% \leqslant PBIAS < \pm25\%$, or $PBIAS \geqslant \pm25\%$, respectively; or by $0.75 < NSE \leqslant 1.0$, $0.65 < NSE \leqslant 0.75$, $0, 0.50 < NSE \leqslant 0.65$, or $NSE \leqslant 0.50$, respectively.

3 Results

3.1 Model calibration and validation

The model parameters, maximum LAI (LAI_{max}), saturated hydraulic conductivities (K_s), and exponent of the soil-water characteristic curve (B), were calibrated and validated using the field measurements. The initial value of the LAI_{max} was assigned a default of 5.0 in the SWAT model; the initial values for K_s and B were based on measurements in the laboratory

of the samples taken from the field site. The soil hydraulic parameters varied for the different soil layers. The calibration was performed manually using the observed LAI and soil water content as the target. The performance was evaluated using the indices mentioned in the previous section, and the calibrated values are listed in **Table S1**.

The simulated LAI values were plotted against the field measurements for 2014–2016 for calibration and 2017–2018 for validation (Fig 5). Further, the MODIS-derived LAI values were used for evaluating the simulation over the entire period as well, especially for the validation period of 2017–2018, for which the field measurements were not available.
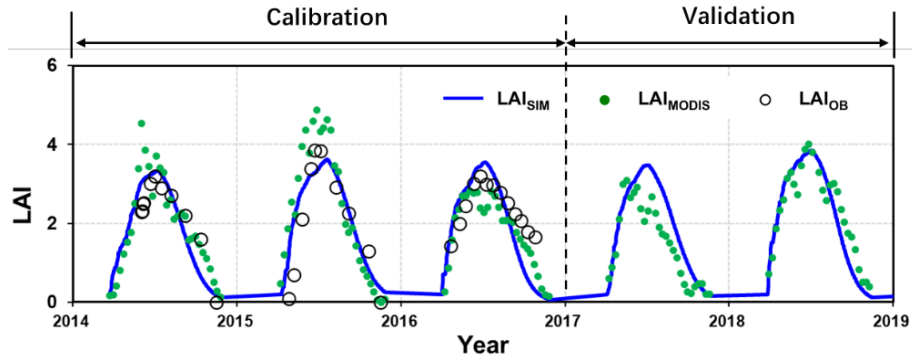
Figure 5: Comparison of leaf area index (LAI) from simulation (LAI$_{SIM}$), MODIS-derived data (LAI$_{MODIS}$), and plot observation (LAI$_{OB}$) for the calibration (2014–2016) and validation (2017–2018) periods.

During the calibration period, the simulated LAI values fit the measurements with a classification of "very good" (Moriasi et al., 2007), with the *NSE* of 0.60 and *PBIAS* of 5.2%. Validation with the MODIS-derived LAI indicated a "very good" performance (Moriasi et al., 2007) with the *NSE* of 0.80 and *PBIAS* of 17.5%.

The MODIS-derived LAI exhibited remarkably similar seasonal patterns to the field measurements. Over- or under-estimation was also noticed, for example, in 2014–2016 and 2017, respectively (Fig 5). Other studies have reported that overestimation may occur especially for the LAI during the wet season when compared with the field experiments (Yang, 2006; Naithani et al., 2013), or cross-evaluated against other remote sensing-based products (Garrigues et al., 2013). The simulation demonstrated an overestimation of LAI when compared with the MODIS-derived LAI in 2017. Although it is also argued that the MODIS-derived LAI may under-estimate the reality (Fang et al., 2012), it is not sure which one (or both) is responsible for the discrepancy between the simulated and observed values in 2017 due to the non-availability of the field measurements. The point-pixel comparison issue might also be a reason for the quantitative difference between the MODIS-derived and field-measured LAI. Nevertheless, the evaluation indices indicate the acceptance of the *LAI$_{max}$* by the model performance in both the calibration and validation stages.

Fig 6 shows a simplified comparison the average soil water content (SWC) over the 5.0 m profile, which illustrates the differences among the root growth simulations. The simulations reproduced the patterns in SWC throughout the seasons and between rainfall events exceptionally well in both the calibration and validation stages. The dynamic fine root distribution

approaches (SD and DD) reproduced the variations in SWC remarkably well; however, the static root distribution (SS) approach deviated significantly. Therefore, the results of this approach will no longer be discussed in the following sections.

380
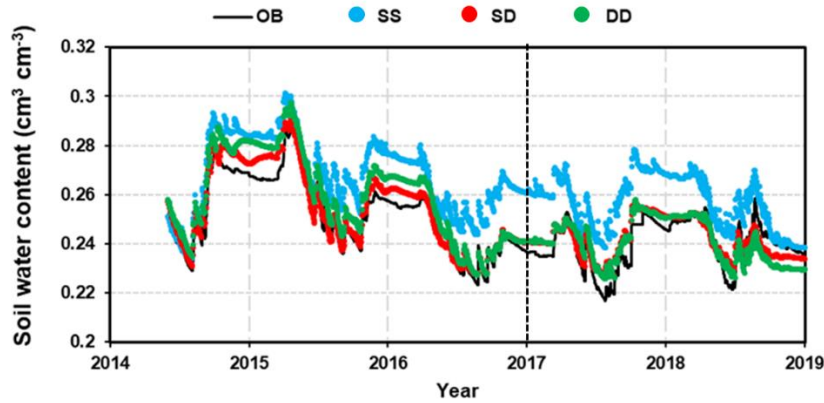
Figure 6: Comparison of the 5 m profile averaged soil water content (SWC) from observation (OB) and three root simulation approaches during the calibration (2014–2016) and validation (2017–2018) period. Notes: SS, Static rooting depth and Static fine root distribution; SD, Static rooting depth and Dynamic fine root distribution; DD, Dynamic rooting depth and Dynamic
385 **distribution of fine roots.**

The evaluation indices R^2 for the static and dynamic rooting depth approaches were 0.96, 0.96, NSE 0.91 and 0.71, and $PBIAS$ 1.2% and 2.9%, respectively, at the calibration stage; R^2 0.66 and 0.64, NSE 0.66 and 0.58, and $PBIAS$ 7.0% and 0.4%, respectively, at the validation stage. The performances can be categorised as "good" or "very good" following the rating system by Moriasi et al. (2007).

390 The fine root density profiles produced during the calibration and validation stages were compared with the sampled values obtained in August 2015 (Fig 7). The measured fine root densities varied significantly among the seven sampled profiles, and the variations decreased with soil depth. The simulated fine root densities exhibited an even wider range of variations, which covered the growth seasons from 2014 to 2018. On average, the root distribution of the dynamic rooting depth approach was closer to the measurements than that of the static rooting depth approach.
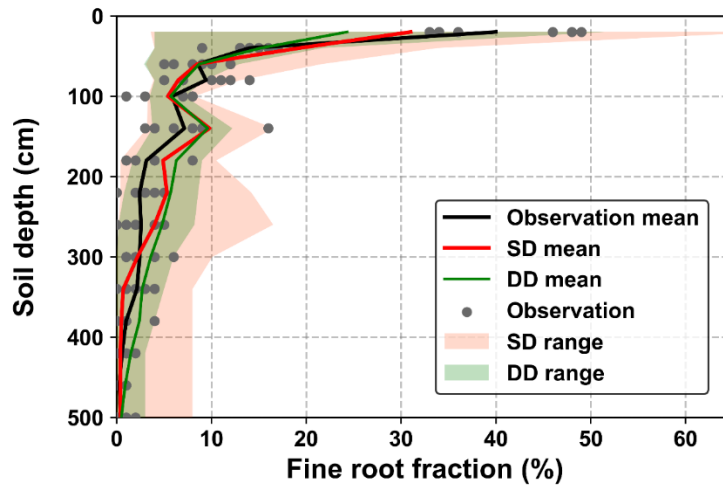
395

Figure 7: Comparison of the 5 m profile averaged soil water content (SWC) from observation (OB) and two root simulation approaches during the calibration (2014–2016) and validation (2017–2018) period. Notes: SD, Static rooting depth and Dynamic fine root distribution; DD, Dynamic rooting depth and Dynamic distribution of fine roots.

Variations in fine root distribution simulated by the static and dynamic rooting depth resulted from strategies for

400   simulating the root–soil water interactions. In the static rooting depth approach, the growth of fine roots was purely

determined by soil water availability and its distribution within the rooting domain, for example, 5.0 m in this study (see Eqs.

(3) and (5) in Section 2.1.4). In contrast, in the dynamic rooting depth approach, growth of the fine roots may demand an

increment of coarse roots that will cost more carbon and is finally determined by the optimisation of the cost-benefit

functions, as described by Eqs. (12) and (18). Thus, the dynamic root depth approach resulted in a narrower variation range

405   than the static rooting depth approach. Averaged over the simulation period, the dynamic rooting depth approach achieved a

more homogeneous fine root distribution profile than the static rooting depth approach, implying that the former approach

utilised more soil water from the deeper soil layers. This point will be further addressed in the discussion regarding the

drying soil layer evolution over the long term.

3.2 Long-term simulation

410   **3.2.1 Rooting depth and soil water**

Simulations forced by the long-term climatic data series revealed root development using the static and dynamic rooting

depth approaches (Fig 8a). Instead of assigning a fixed root depth of 5.0 m in the static rooting depth approach, the dynamic

rooting depth approach simulated the root depth extension, which is consistent with the data from the literature. It was found

that the rooting depth may be as deep as 11.0 m below the ground. The simulated rooting depth extension rate slowed as the

415   stand age increased, which was also consistent with the observations in artificial forests (Christina et al., 2011; Wang et al.,

2015) (see in **Fig S4).** Furthermore, the simulated root profiles by the two approaches within a 2.0 m soil depth were also

evaluated against the data collected from the literature (Fig 8b&c). The simulated results varied within the range provided by the data in the literature. Regressions between the mean fine root fractions by the static and dynamic rooting depth approaches and that of the literature data provided R^2 values of 0.34 and 0.64, respectively, indicating that the dynamic approach performed better than the static approach.
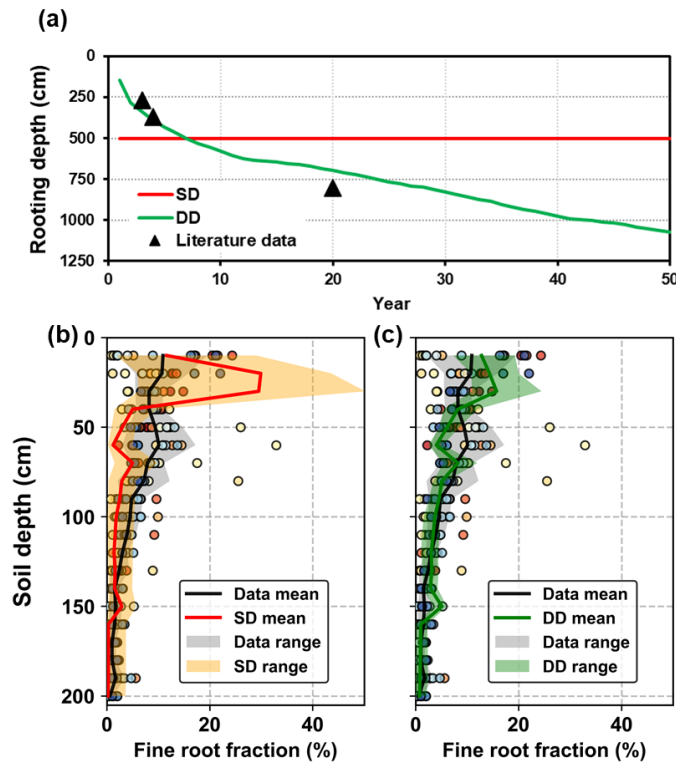
Figure 8: Evaluation of the simulated root distribution against the literature data. (a) Rooting depth, (b) fine root distribution in top 2.0 m soil layer for the static rooting depth approach (SD), (c) fine root distribution in top 2.0 m soil layer for the dynamic rooting depth approach (DD). The scatters with different colours illustrate the observational data from different literature, and the shaded areas illustrate the range of mean ± standard deviation of simulation.

The evolution of root growth and soil water over the long term is depicted in Fig 9. Visually, wetting and drying processes over the soil profiles were commonly found from simulations of both root growth modelling approaches. However, the difference in the simulated soil water distribution was also significant (Fig 9d).
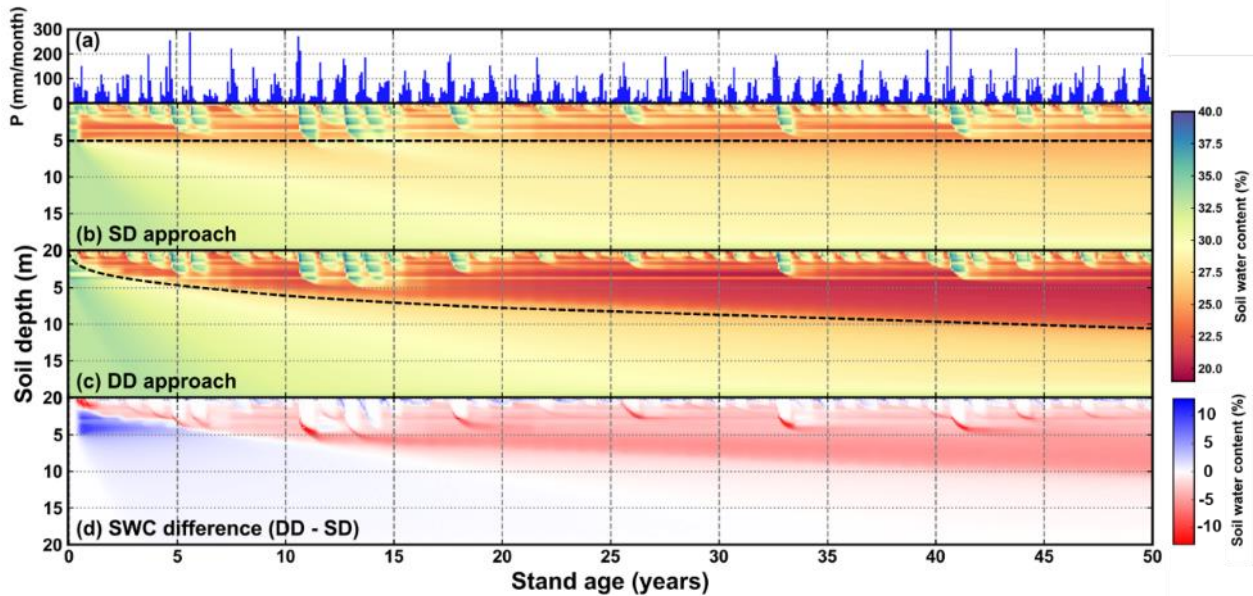
Figure 9: Time series of (a) monthly precipitation (mm month[-1]), (b) soil water content (SWC) along the 20 m soil profile simulated by the static rooting depth (SD) approach, (c) soil water content along the 20 m soil profile simulated by the dynamic rooting depth (DD) approach, (d) the difference of SWC between the SD and DD approaches. The dashed black horizontal line in (b) and curve in (c) indicate the rooting depth.

These two approaches resulted in substantially different spatial distributions of roots and soil water, and thus a significant difference in root–water interactions. The soil water varied significantly with precipitation during the entire period. In most years, the maximum infiltration depth was less than 2.0 m. Meanwhile, precipitation could infiltrate down to 5.0 m in consecutive wet years, for example, the period from the 10th to 15th years. Notably, a time lag effect existed between the peak precipitation and the maximum infiltration depth; the peak precipitation occurred around August, while the maximum infiltration depth was reached around March in the following year.

3.2.2 Infiltration

Precipitation replenishes soil water through infiltration. The amount and depth of the infiltrated water impact the growth and water use of the root systems. The infiltration is associated with the a priori soil water content and its distribution over the profile, the amount and duration of an individual precipitation event, and the effects of the randomly sequential events. Establishing a relationship between the infiltration depth and precipitation on the basis of a single event is complicated and difficult to achieve. Instead, analyses were performed on an annual basis, that is, the maximum infiltration depth vs. the annual precipitation amount were regressed for the two root growth modelling approaches, as shown in Fig 10. During the simulation period of 50 years, the annual precipitation varied from 250 to 850 mm. It was found that the annual infiltration amounts by these two approaches were exceptionally close to each other. The dynamic rooting depth approach was 4.0%

lower than that of the static rooting depth approach, which is an insignificant difference, as discussed in a later section. The

450 maximum infiltration depth was positively correlated with the annual precipitation, which is not uncommon. The results also indicate that the maximum infiltration depth may reach 6.0 m below the ground in the very wet years. Interestingly, the regression lines of these two root growth modelling approaches crossed at approximately 500 mm of annual precipitation. When annual precipitation was less than 500 mm, the infiltration reached deeper soil for the static rooting depth approach, and vice versa when the annual precipitation was more than 500 mm.
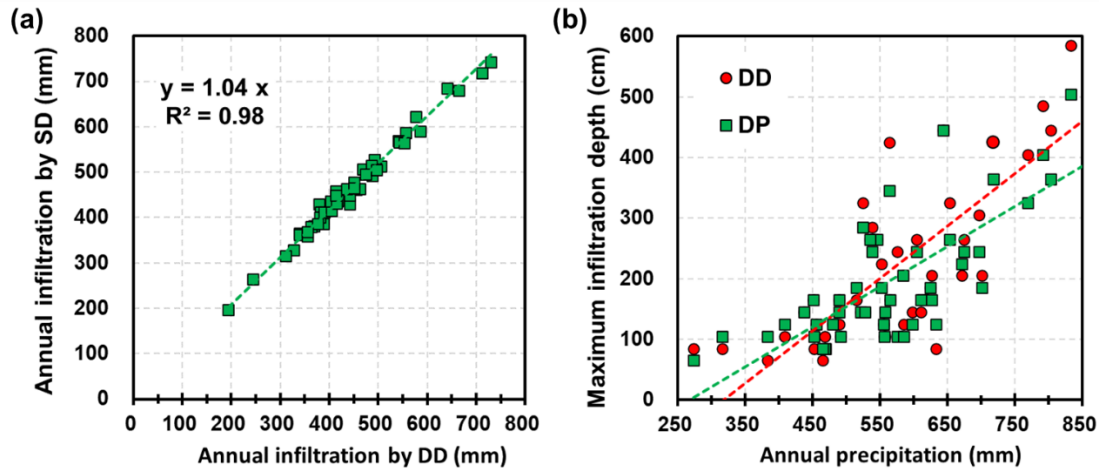
455

Figure 10: Comparisons of (a) infiltration amounts and (b) maximum infiltration depths between the static rooting depth (SD) and dynamic rooting depth (DD) approaches

3.2.3 Fine root distribution and water uptake

The fine root distributions simulated by these two approaches showed exceptionally similar patterns in the soil profile (Fig

460 11a). However, a quantitative difference between them was also noticeable. For the static rooting depth approach, roots grow only within the soil layer with a present 5.0 m thickness. For the dynamic rooting depth approach, the coarse roots reach 11.0 m below the ground. Within the top 2.0 m soil layer, the fractions of fine roots for the static and dynamic rooting depth approaches were 90.0% and 80.3%, respectively, and within the 2.0–5.0 m soil layer, 10.0% and 14.7%, respectively. For the dynamic rooting depth approach, only 5.0% of fine roots were in the soil below 5.0 m.
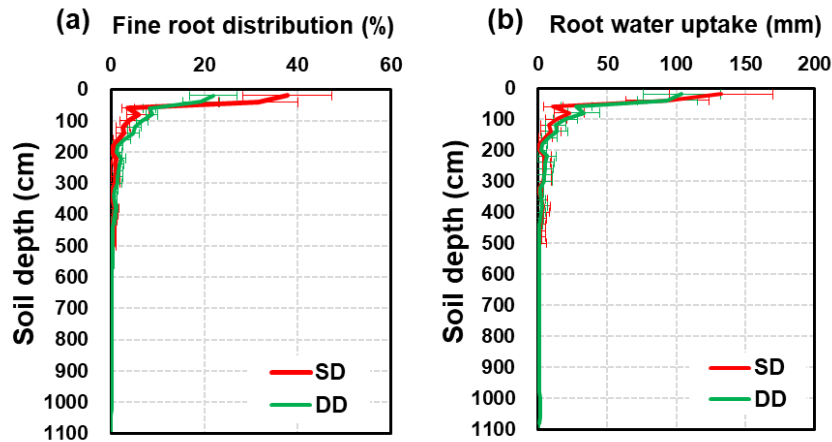
465

Figure 11: Profile of (a) fine root density distributions (%) and (b) root water uptake distributions (mm) resulting from different approaches (SD and DD approach). The error bars represent the standard error (STD) of the mean of different years.

The distribution of root water uptake over the soil profile was similar to that of the fine root density (Fig 11b). The static rooting depth approach resulted in an annual water uptake of 338 mm (STD = 84 mm), while the dynamic rooting depth

470 approached 381 mm (STD = 84 mm). In the top 2.0 m soil layer, the root uptake was 298 mm and 318 mm for the static and dynamic rooting depth approaches, respectively; 40 mm and 40 mm, respectively, in the 2.0–5.0 m layer. Below 5.0 m, the dynamic approach resulted in a root uptake of 24 mm, which accounted for 6.2% of the uptake from the entire profile.

3.2.4 Evolution of drying soil layers

The long-term soil water evolution is illustrated in Fig 9. Vertically, the most active soil water zone was within the top 2.0

475 m, statistically based on the simulation results. This was confirmed by root development and water uptake in this study (Fig 11) and by field observations in this region (Suo et al., 2018). In the top 2.0 m soil layer, infiltration events replenish and plant roots deplete the soil water alternately. The two root growth modelling approaches resulted in remarkably similar soil water enrichment and depletion patterns in the top 2.0 m layer, especially during the infiltration period (Fig. 9d). Below the top 2.0 m, soil water was continuously in a negative state, and the dynamic rooting depth approach resulted in more soil

480 water depletion than the static rooting depth approach.

Drying soil layers have been frequently reported in previous studies in the Loess Plateau (Wang et al., 2018b). The upper and lower boundaries of the drying soil layers were defined according to the soil desiccation index (Wang et al., 2011), as shown in Fig 12. The static rooting depth approach did not demonstrate the sustainable existence of the drying soil layers. This is because it pre-sets a fixed rooting depth over the simulation period, which does not capture the hydraulic traits of

485 roots that may develop to use water from the wetter zone beneath the pre-set rooting depth.

For the dynamic rooting depth approach, the drying soil layers started to develop at a stand age of approximately 8 years and became deeper and thicker sustainably with the increasing stand age. Its lower boundary extended gradually to deeper

soil, while its upper boundary fluctuated significantly. The strong fluctuations were associated with the infiltration, while the continuous extension of the lower boundary was due to sustained plant root uptake and rare recharge. With the stand aging, the soil water content in the drying soil layer decreased continuously, and the thickness increased gradually.
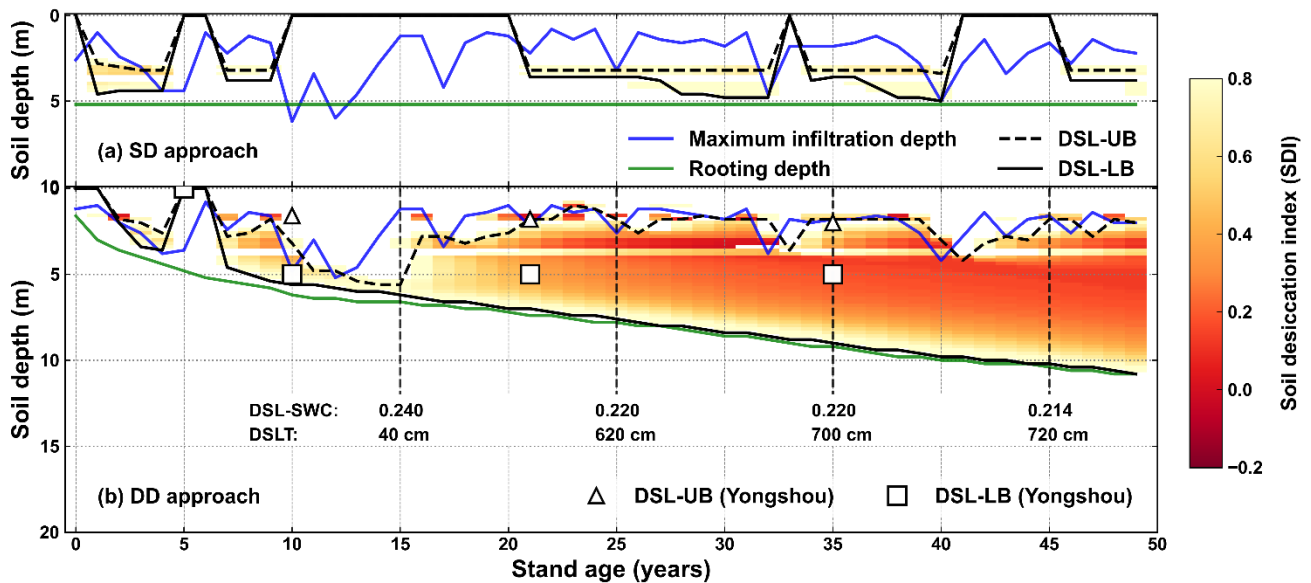
Figure 12: Evolution of the drying soil layers with stand age simulated by (a) the static rooting depth (SD) and (b) the dynamic rooting depth (DD) approaches over a 50-year period at Yongshou, Loess Plateau. The triangles and squares are the observed upper and lower boundaries, respectively, adopted from Jia et al. (2017a). Notes: DSL-UB: the upper boundary of drying soil layer; DSL-LB: the lower boundary of drying soil layer; DSL-SWC: mean soil water content within the drying soil layer; DSLT: the thickness of the drying soil layer.

The simulated evolution of the drying soil layers was partially confirmed by field observations (Jia et al., 2017a), as shown in Fig 12. The simulation produced a progressive course of the lower boundary, which was far deeper below the ground than the observations. The observations were limited to the top 5.0 m only. A deeper sampling might have resulted in a thicker drying soil. In Changwu, which is 80 km away from the study site in the Loess Plateau, it was reported that the thickness of the drying soil layer reached 7.0 m, with its lower boundary as deep as 8.0 m below the ground in the black locust plantation (Li et al., 2008). It should also be noted that the sampling depth was limited at 8.0 m. Deep samplings have indicated that the drying soil layers reached the depth of 19.0 m in the Loess Plateau (Wu et al., 2021).

4 Discussion

4.1 Root–water interactions and drying soil layers

As indicated in the introduction section, this study attempted to develop a root growth model that can simulate coarse root extension dynamically instead of the static rooting depth approach currently adopted in most available models (Sivandran and Bras, 2013; Wang et al., 2016; Wang et al., 2018a; Drewniak, 2019; Niu et al., 2020). In formulating the dynamic rooting depth, the study proposed a cost–benefit algorithm based on ecophysiological principles (Chen et al., 2019). The evaluation of the simulated results against the field observations from this study and from the literature proved its effectiveness for the Loess Plateau.

The static rooting depth approach is widely used in ecological and hydrological models, which have been used to simulate soil water variations in field crops, shrubs, and forests in the Loess Plateau (Zhang et al., 2015; Tian et al., 2016; Li et al., 2017; Bai et al., 2020). Short-term model calibration and validation, ranging from months to five years, has usually shown acceptable performance, while long-term evaluation has rarely been undertaken. When used to address the long-term issue in this study, comparisons between the static and dynamic rooting depth approaches indicated that the former did not reproduce the occurrence and evolution of the drying soil layers due to its pre-set rooting depth (Fig 12). The drying soil layers simulated by the static approach were discontinuous along the soil profile (**Fig S5**), due to sufficient precipitation infiltration recharging the soil moisture during the humid period. Meanwhile, the lower boundary of the drying soil layers was less than 5.0 m, which was constrained by the fixed tree rooting depth. These results are inconsistent with the actual conditions observed by deep samplings in this region, which indicated a deeper, continuous drying soil layer (Wang et al., 2013; Zhao et al., 2019). Therefore, the static rooting depth approach reflected neither the change of soil moisture in the deeper layer (>5.0 m) nor the evolution of the drying soil layers, as it did not allow for the deeper water uptake by roots.

Notably, the development of the drying soil layers is predominantly due to water utilisation by the deep fine roots, which accounts for approximately only 5% of the total profile uptake (Fig 11). Although minor compared with the total, it caused a sustained negative soil water balance in the deep soil due to difficulties in receiving recharge, as described in the results section. The continuous development of the lower boundary of the drying soil layer implies that its recovery is critically difficult. This is because of the large thickness and vast storage capacity of loess soil (Huang and Shao, 2019). Plants tend to develop more fine roots in the topsoil and use more soil water due to lower costs but higher benefits, that is, a more profitable adaptation strategy when experiencing water stress. Exploration of water from wetter but deeper soil is also an adaption strategy when it is more profitable, but deep roots might be more expensive to construct and maintain (Pierret et al., 2016; Germon et al., 2020). This explains why the top 2.0 m soil was the most active zone of water uptake in this study. Depletion of topsoil always vacates the storage for infiltration, making it difficult for the rainfall to replenish the deeper dried soil layer or groundwater (Turkeltaub et al., 2018).

The occurrence and development of the drying soil layer significantly impact plant–water relationship and the local hydrological cycling in the Loess Plateau, where the combination of deep loess soil and the semiarid and arid climate prevails (Zhao et al., 2019). This might also be an issue in other regions with similar soil and climate conditions (Shao et al., 2018); in fact, this phenomenon has also been reported elsewhere, such as in the Amazonia forest (Jipp et al., 1998) and southern Australia dryland (Robinson et al., 2006), due to artificial afforestation. The occurrence of the persistent drying soil layer not only degrades soil and vegetation, but also negatively impacts ecosystem functions and services (Huang and Shao, 2019), such as the premature of the artificially planted trees (Jia et al., 2017a). The drying soil layer and the degraded artificial afforestation are believed mutually causative. The long-term simulation results also affirm the importance of monitoring both the long-term vegetation and soil water dynamics of the artificial forests for the ecosystem restoration practices in the Loess Plateau, for example, the Grain−for-Green Project implemented in 1999.

4.2 Outlooks of future work

Roots develop beneath the ground, which is widely accepted to be critically difficult to monitor; the deeper the soil depth, the harder it is to sample (Maeght et al., 2013; Warren et al., 2015; Fan et al., 2017). Observations of the rooting depths are rarely available for ready use, especially the knowledge of the maximum rooting depth for vegetation in a region. Occasionally, the limited data may provide a rough estimate, for example, Li et al. (2019) and Wu et al. (2021) reported some maximum rooting depths of black locust and apple trees of approximately 25.0 m (Li et al., 2019b; Wu et al., 2021). Mathematical simulation is a beneficial compensation for field observations and can go far beyond its limitations, although its effectiveness relies on the actual data. The simulation can reproduce the dynamics of roots at very fine temporal and spatial resolutions, while *in situ* data are usually extremely rare. This study adopted *in situ* data at only a single moment, as shown in Fig 3. Fortunately, it was found that the measurements fell within the variation range of the simulations over some time periods, which is understandable from the statistical point of view. *In situ* data are believed to remain an issue in the development and evaluation of root approaches in the long term (Pierret et al., 2016).

The simulation results indicated that the annual infiltration amount by the static rooting depth approach was 4.0% higher than that of the dynamic rooting depth approach (Fig 10). In the field, no surface runoff was found during the years of observation at the study site at Yeheshan. The minor difference in the infiltration amount between these two rooting depth approaches was due to canopy interception. The static rooting depth approach limits the roots to develop and use water within the top 5.0 m soil layer, while the dynamic rooting depth approach permits the root to grow into deep wetter soil for uptake, which can release more soil water stress. The lower the soil water stress, the greater the leaf area and canopy storage. This small difference in the infiltration amount between these two approaches highlights the internal relationship between the above and belowground parts of the plants. The allocation of biomass between the above and belowground parts changes with climate, soil water, and nutrients over time and varies among vegetation types (Pooter et al., 2012; Qi et al., 2019). These mechanisms were involved in the model of this study. However, this study adopted a fixed allocation factor, to focus

on investigating the temporal and spatial changes in the rooting depth, fine root distribution, and their impacts on soil water evolution over the long term. Further attempts will be made to investigate the systematic behaviour of the plants on their adaptation strategies to obtain the maximum cost-benefit ratio by optimising the biomass allocation between the above and belowground parts via a trade-off strategy (Trugman et al., 2019; Sakschewski et al., 2021) and the spatial distribution of roots over the soil profile.

5 Conclusion

The study established a plant model and used it to investigate plant–water interactions in the Loess Plateau. This paper presents the results focusing on the root growth model and root–water interactions. The results indicate that incorporating the dynamic rooting depth into the currently available root growth model is a necessary step for an in-depth understanding of the occurrence and evolution of the widely reported drying soil layer phenomena in this region, which has also been reported elsewhere.

The model provided a much more powerful tool to address the drying soil layer issue than *in situ* sampling techniques. It was found that the lower boundary of the drying soil layer extended sustainably due to the rare chances of replenishment by rainfall, while its upper boundary fluctuated strongly with the infiltration events. Continuous extension of the thickness of the drying soil layer and the difficulties in recovery may have strong implications for forest–water management in this region.

Code and data availability.

585 The meteorological datasets are available at http://data.cma.cn. The literature data datasets are available at in supplementary excel files. Further datasets and model code can be accessed upon request to the corresponding author.

Author Contributions.

Conceived and designed the research: YL and LS. Performed the experiments: HL, LS and XL. Collected and analysed the data: HL, XL, CM, TJ and HZ. Wrote and edited the paper: HL, YL and XW.

590 **Competing interests.**

The authors declare that they have no conflict of interest.

Acknowledgement

This work was supported by the National Key Research and Development Plan of China (NO. 2016YFC0501603) and the National Natural Science Foundation of China (NO. 41390461 and 41571130081). We also thank Dr. Jian Shi from Institute

595 of Automation, Chinese Academy of Sciences, for his help for root image analysis. We would like to thank the anonymous reviewers of this paper for their helpful comments and suggestions.

References

Arnold, J.G., D.N. Moriasi, P.W. Gassman, K.C. Abbaspour, M.J. White, R., and Srinivasan, C. et al.: SWAT: Model use, calibration, and validation, Trans. ASABE, 55(4), 1491-1508, doi: 10.13031/2013.42256, 2012.

600 Bai, X., Jia, X., Jia, Y., Shao, M. and Hu, W.: Modeling long-term soil water dynamics in response to land-use change in a semi-arid area, J. Hydrol., 585, 124824, doi:10.1016/j.jhydrol.2020.124824, 2020.

Bardgett, R.D., Mommer, L. and De Vries, F.T.: Going underground: root traits as drivers of ecosystem processes, Trends Ecol. Evol., 29(12), 692-699, doi:10.1016/j.tree.2014.10.006, 2014.

Brunner, I., Herzog, C., Dawes, M.A., Arend, M. and Sperisen, C.: How tree roots respond to drought, Front Plant Sci., 6,

605 547-547, doi:10.3389/fpls.2015.00547, 2015.

Carlson, W. C., and Harrington, C. A.: Cross-sectional area relationships in root systems of loblolly and shortleaf pine, Can. J. For. Res., 17(6), 556–558, doi:10.1139/x87-092, 1987.

Chen, G., Hobbie, S.E., Reich, P.B., Yang, Y. and Robinson, D.: Allometry of fine roots in forest ecosystems, Ecol. Lett., 22(2), 322-331, doi:10.1111/ele.13193, 2019.

610 Collins, D.B.G. and Bras, R.L.: Plant rooting strategies in water-limited ecosystems, Water Resour. Res., 43(6), W06407, doi:10.1029/2006WR005541, 2007.

Christina, M., Laclau, J., Gonçalves, J., Jourdan, C., Nouvellon, Y., and Bouillet, J.: Almost symmetrical vertical growth rates above and below ground in one of the world's most productive forests, Ecosphere, 2(3), 1-10, doi:10.1890/ES10-00158.1, 2011.

615   Christina, M., Nouvellon, Y., Laclau, J., Stape, J., Bouillet, J., Lambais, G., & Maire, G.: Importance of deep water uptake in tropical eucalypt forest, Funct Ecol, 31(2), 509-519, doi:10.1111/1365-2435.12727, 2017.

Clark, M., Fan, Y., Lawrence, D., Adam, J., Bolster, D., and Gochis, D. et al.: Improving the representation of hydrologic processes in Earth System Models, Water Resour. Res., 51(8), 5929-5956, doi:10.1002/2015WR017096, 2015.

Demarez, V., Duthoit, S., Baret, F., Weiss, M., and Dedieu, G.: Estimation of leaf area and clumping indexes of crops with

620   hemispherical photographs, Agric. For. Meteorol., 148(4), 644–655, doi:10.1016/j.agrformet.2007.11.015, 2008.

Deng, L., Yan, W.M., Zhang, Y.W. and Shangguan, Z.P.: Severe depletion of soil moisture following land-use changes for ecological restoration: Evidence from northern China, Forest Ecol. Manag., 366, 1-10, doi:10.1016/j.foreco.2016.01.026, 2016.

Drewniak, B.A.: Simulating Dynamic Roots in the Energy Exascale Earth System Land Model, J. Adv. Model. Earth Syst.,

625   11(1), 338-359, doi:10.1029/2018MS001334, 2019.

Fan, Y., Miguez-Macho, G., Jobbagy, E.G., Jackson, R.B. and Otero-Casal, C.: Hydrologic regulation of plant rooting depth, P. Natl. Acad. Sci. USA, 114(40), 10572-10577, doi:10.1073/pnas.1712381114, 2017.

Fang, H., Wei, S. and Liang, S.: Validation of MODIS and CYCLOPES LAI products using global field measurement data, Remote Sens. Environ., 119(1), 43-54, doi:10.1016/j.rse.2011.12.006, 2012.

630   Feddes, R., Hoff, H., Bruen, M., Dawson, T., de Rosnay, P., and Dirmeyer, P. et al.: Modeling root water uptake in hydrological and climate models, Bull. Amer. Meteorol. Soc., 82(12), 2797-2809, doi:10.1175/1520-0477(2001)082%3C2797:MRWUIH%3E2.3.CO;2, 2001.

Garrigues, S., Lacaze, R., Baret, F., Morisette, J., Weiss, M., and Nickeson, J. et al.: Validation and intercomparison of global Leaf Area Index products derived from remote sensing data, J. Geophys. Res.-Biogeosci., 113, G02028,

635   doi:10.1029/2007JG000635, 2008.

Gayler, S., Wöhling, T., Grzeschik, M., Ingwersen, J., Wizemann, H., and Warrach-Sagi, K. et al.: Incorporating dynamic root growth enhances the performance of Noah-MP at two contrasting winter wheat field sites, Water Resour. Res., 50(2), 1337-1356, doi:10.1002/2013WR014634, 2014.

Germon, A., Laclau, J.P., Robin, A. and Jourdan, C.: Tamm Review: Deep fine roots in forest ecosystems: Why dig deeper?

640   Forest Ecol. Manag., 466, 118135, doi:10.1016/j.foreco.2020.118135, 2020.

Guswa, A.J., 2008. The influence of climate on root depth: A carbon cost-benefit analysis, Water Resour. Res., 44(2), W02427, doi:10.1029/2007WR006384, 2008.

Han, X., Franssen, H., Montzka, C. and Vereecken, H.: Soil moisture and soil properties estimation in the Community Land Model with synthetic brightness temperature observations, Water Resour. Res., 50(7), 6081-6105,

645   doi:10.1002/2013WR014586, 2014.

Hashemian, M., Ryu, D., Crow, W.T. and Kustas, W.P.: Improving root-zone soil moisture estimations using dynamic root growth and crop phenology, Adv. Water Resour., 86, 170-183, doi:10.1016/j.advwatres.2015.10.001, 2015.

Huang, L. and Shao, M.A.: Advances and perspectives on soil water research in China's Loess Plateau, Earth-Sci. Rev., 199, 102962, doi:10.1016/j.earscirev.2019.102962, 2019.

650 Ivanov, V., Hutyra, L., Wofsy, S., Munger, J., Saleska, S., de Oliveira, R., and de Camargo, P.: Root niche separation can explain avoidance of seasonal drought stress and vulnerability of overstory trees to extended drought in a mature Amazonian forest, Water Resour. Res., 48(12), W12507, doi:10.1029/2012WR011972, 2012.

Jackson, R., Canadell, J., Ehleringer, J., Mooney, H., Sala, O., and Schulze, E.: A global analysis of root distributions for terrestrial biomes, Oecologia, 108(3), 389-411, doi:10.1007/BF00333714, 1996.

655 Jia, X., Shao, M., Zhu, Y. and Luo, Y.: Soil moisture decline due to afforestation across the Loess Plateau, China, J. Hydrol., 546, 113-122, doi:10.1016/j.jhydrol.2017.01.011, 2017a.

Jia, X., Shao, M., Yu, D., Zhang, Y., and Binley, A.: Spatial variations in soil-water carrying capacity of three typical revegetation species on the Loess Plateau, China, Agric. Ecosyst. Environ., 273, 25–35, doi:10.1016/j.agee.2018.12.008, 2019.

660 Jia, X., Wang, Y., Shao, M., Luo, Y. and Zhang, C.C.: Estimating regional losses of soil water due to the conversion of agricultural land to forest in China's Loess Plateau, Ecohydrology, 10(6), e1851, doi:10.1002/eco.1851, 2017b.

Jipp, P.H., Nepstad, D.C., Cassel, D.K. and De Carvalho, C.R.: Deep soil moisture storage and transpiration in forests and pastures of seasonally-dry Amazonia, Clim. Change, 39(2-3), 395-412, doi:10.1023/A:1005308930871,1998.

Jonckheere, I., Fleck, S., Nackaerts, K., Muys, B., Coppin, P., Weiss, M., and Baret, F.: Review of methods for in situ leaf
665 area index determination - Part I. Theories, sensors and hemispherical photography, Agric. For. Meteorol., 121(1-2), 19-35, doi:10.1016/j.agrformet.2003.08.027, 2004.

Kleidon, A. and Heimann, M.: A method of determining rooting depth from a terrestrial biosphere model and its impacts on the global water and carbon cycle, Glob. Change Biol., 4(3), 275–286, doi:10.1046/j.1365-2486.1998.00152.x, 1998.

Knighton, J., Singh, K. and Evaristo, J.: Understanding Catchment-Scale Forest Root Water Uptake Strategies Across the
670 Continental United States Through Inverse Ecohydrological Modeling, Geophys. Res. Lett., 47(1), e2019GL085937, doi:10.1029/2019GL085937, 2020.

Lehnebach, R., Beyer, R., Letort, V. and Heuret, P.: The pipe model theory half a century on: a review, Ann. Bot., 121(5), 773-795, doi:10.1093/aob/mcy031, 2018.

Li, B., Wang, Y., Hill, R.L. and Li, Z.: Effects of apple orchards converted from farmlands on soil water balance in the deep
675 loess deposits based on HYDRUS-1D model, Agric. Ecosyst. Environ., 285, 106645, doi:10.1016/j.agee.2019.106645, 2019a.

Li, H., Si, B., Wu, P. and McDonnell, J.J.: Water mining from the deep critical zone by apple trees growing on loess, Hydrol. Process., 33(2), 320-327, doi:10.1002/hyp.13346, 2019b.

Li, J., Chen, B., Li, X., Zhao, Y., Ciren, Y., and Jiang, B., et al.: Effects of deep soil desiccation on artificial forestlands in
680   different vegetation zones on the Loess Plateau of China, Acta Ecol. Sin., 28(4), 1429-1445, doi:10.1016/S1872-2032(08)60052-9, 2008.

Liang, H., Xue, Y., Li, Z., Wang, S., Wu, X., and Gao, G. et al.: Soil moisture decline following the plantation of *Robinia pseudoacacia* forests: Evidence from the Loess Plateau, Forest Ecol. Manag., 412, 62-69, doi:10.1016/j.foreco.2018.01.041, 2018.

685   Liu, B. and Shao, M.: Modeling soil-water dynamics and soil-water carrying capacity for vegetation on the Loess Plateau, China, Agr. Water Manage., 159, 176-184, doi:10.1016/j.agwat.2015.06.019, 2015.

Liu, W., Zhang, X., Dang, T., Ouyang, Z., Li, Z., and Wang, J. et al.: Soil water dynamics and deep soil recharge in a record wet year in the southern Loess Plateau of China, Agric. Water Manage., 97(8), 1133-1138, doi:10.1016/j.agwat.2010.01.001, 2010.

690   Liu, X., Chen, F., Barlage, M. and Niyogi, D.: Implementing Dynamic Rooting Depth for Improved Simulation of Soil Moisture and Land Surface Feedbacks in Noah-MP-Crop, J. Adv. Model. Earth Syst., 12(2), e2019MS001786, doi:10.1029/2019MS001786, 2020.

Luo, Y., OuYang, Z., Yuan, G., Tang, D. and Xie, X.: Evaluation of macroscopic root water uptake models using lysimeter data, Trans. ASAE, 46(3), 625-634, doi: 10.13031/2013.13598, 2003.

695   Ma, C., Luo, Y., Shao, M., Li, X., Sun, L., and Jia, X.: Environmental controls on sap flow in black locust forest in Loess Plateau, China. Sci. Rep., 7(1): 13160-13160, doi:10.1038/s41598-017-13532-8, 2017.

Maeght, J.L., Rewald, B. and Pierret, A.: How to study deep roots - and why it matters, Front. Plant Sci., 4, 299, doi:10.3389/fpls.2013.00299, 2013.

Mencuccini, M., Manzoni, S. and Christoffersen, B.: Modelling water fluxes in plants: from tissues to biosphere. New
700   Phytol., 222, 3, 1207-1222, doi:10.1111/nph.15681, 2019.

Moriasi, D., Arnold, J., Van Liew, M., Bingner, R., Harmel, R. and Veith. T.: Model evaluation guidelines for systematic quantification of accuracy in watershed simulations, Trans. ASABE, 50(3): 885-900, doi:10.13031/2013.23153, 2007.

Mulia, R. and Dupraz, C.: Unusual fine root distributions of two deciduous tree species in southern France: What consequences for modelling of tree root dynamics? Plant Soil, 281, 1-2, 71-85, doi:10.1007/s11104-005-3770-6, 2006.

705   Naithani, K.J., Baldwin, D.C., Gaines, K.P., Lin, H., and Eissenstat, D.M.: Spatial distribution of tree species governs the spatio-temporal interaction of leaf area index and soil moisture across a forested landscape, PLoS One, 8, 3, 1–12, doi:10.1371/journal.pone.0058704, 2013.

Neitsch, S.L., Arnold, J.G., Kiniry, J.R. and Williams, J.R.: Soil and Water Assessment Tool: Theoretical Documentation—Version 2009. Texas Water Resources Institute Technical Report No. 406. Agricultural Research Service (USDA) & Texas
710   Agricultural Experiment Station, Texas A&M University, Temple, 2011.

Nippert, J.B. and Holdo, R.M.: Challenging the maximum rooting depth paradigm in grasslands and savannas, Funct. Ecol., 29,6, 739-745, doi:10.1111/1365-2435.12390, 2015.

Niu, G., Fang, Y., Chang, L., Jin, J., Yuan, H., and Zeng, X.: Enhancing the Noah-MP Ecosystem Response to Droughts With an Explicit Representation of Plant Water Storage Supplied by Dynamic Root Water Uptake, J. Adv. Model. Earth Syst., 12, 11, doi:10.1029/2020MS002062, 2020.

Oleson, K. et al.: Technical description of version 4.5 of the Community Land Model (CLM), UCAR/NCAR, doi:10.5065/D6RR1W7M, 2013.

Ostle, N. J., Smith, P., Fisher, R., Ian Woodward, F., Fisher, J. B., and Smith, J. U. et al.: Integrating plant-soil interactions into global carbon cycle models, J. Ecol., 97(5), 851-863, doi:10.1111/j.1365-2745.2009.01547.x, 2009.

Phillips, R. P., Ibáñez, I., D'Orangeville, L., Hanson, P. J., Ryan, M. G., and McDowell, N. G.: A belowground perspective on the drought sensitivity of forests: Towards improved understanding and simulation, Forest Ecol. Manag., 380, 309-320, doi:10.1016/j.foreco.2016.08.043, 2016.

Pierret, A., Maeght, J.-L., Clément, C., Montoroi, J.-P., Hartmann, C., and Gonkhamdee, S.: Understanding deep roots and their functions in ecosystems: an advocacy for more unconventional research, Ann. Bot., 118(4), 621-635, doi:10.1093/aob/mcw130, 2016.

Pinheiro, R. C., de Deus, J. C., Jr., Nouvellon, Y., Campoe, O. C., Stape, J. L., and Aló, L. L., et al.: A fast exploration of very deep soil layers by Eucalyptus seedlings and clones in Brazil, Forest Ecol. Manag., 366, 143-152, doi:10.1016/j.foreco.2016.02.012, 2016.

Poorter, H., Niklas, K. J., Reich, P. B., Oleksyn, J., Poot, P., and Mommer, L.: Biomass allocation to leaves, stems and roots: meta-analyses of interspecific variation and environmental control, New Phytol., 193, 30–50, 10.1111/j.1469-8137.2011.03952.x, 2012.

Qi, Y., Wei, W., Chen, C., and Chen, L.: Plant root-shoot biomass allocation over diverse biomes: a global synthesis, Glob. Ecol. Conserv., 18, e00606, 10.1016/j.gecco.2019.e00606, 2019.

Qiao, J., Y. Zhu, X. Jia, L. Huang, and M. Shao.: Factors that influence the vertical distribution of soil water content in the Critical Zone on the Loess Plateau, China, Vadose Zone J, 17, 170196, 10.2136/vzj2017.11.0196, 2018.

Ramos, T.B., Simionesei, L., Jauch, E., Almeida, C. and Neves, R.: Modelling soil water and maize growth dynamics influenced by shallow groundwater conditions in the Sorraia Valley region, Portugal, Agric. Water Manage., 185, 27-42, 10.1016/j.agwat.2017.02.007, 2017.

Renton, M. and Poot, P.: Simulation of the evolution of root water foraging strategies in dry and shallow soils, Ann. Bot., 114(4), 763-778, 10.1093/aob/mcu018, 2014.

Richardson, A. D., and Dohna, H. Z.: Predicting root biomass from branching patterns of Douglas-fir root systems, Oikos, 100(1), 96–104, 10.1034/j.1600-0706.2003.12081.x, 2003.

Robinson, N., Harper, R., Smettem, K.: Soil water depletion by Eucalyptus spp. integrated into dryland agricultural systems, Plant Soil, 286(1), 141–151, 10.1007/s11104-006-9032-4, 2006.

745 Rudd, K., Albertson, J.D. and Ferrari, S.: Optimal root profiles in water-limited ecosystems, Adv. Water Resour., 71, 16-22, 10.1016/j.advwatres.2014.04.021, 2014.

Sakschewski, B., von Bloh, W., Drüke, M., Sörensson, A. A., Ruscica, R., Langerwisch, F., Billing, M., Bereswill, S., Hirota, M., Oliveira, R. S., Heinke, J., & Thonicke, K.: Variable tree rooting strategies are key for modelling the distribution, productivity and evapotranspiration of tropical evergreen forests. Biogeosciences, 18(13), 4091–4116, doi: 10.5194/bg-18-

750 4091-2021, 2021.

Schenk, H.J. and Jackson, R.B.: Rooting depths, lateral root spreads and below-ground/above-ground allometries of plants in water-limited ecosystems, J. Ecol., 90(3), 480-494, doi:10.1046/j.1365-2745.2002.00682.x, 2002.

Schymanski, S.J., Sivapalan, M., Roderick, M.L., Beringer, J. and Hutley, L.B.: An optimality-based model of the coupled soil moisture and root dynamics, Hydrol. Earth. Syst. Sc., 12(3), 913-932, doi:10.5194/hess-12-913-2008, 2008.

755 Schymanski, S.J., Sivapalan, M., Roderick, M.L., Hutley, L.B. and Beringer, J.: An optimality-based model of the dynamic feedbacks between natural vegetation and the water balance, Water Resour. Res., 45, W01412, doi:10.1029/2008WR006841, 2009.

Sivandran, G. and Bras, R.L.: Identifying the optimal spatially and temporally invariant root distribution for a semiarid environment, Water Resour. Res., 48, W12525, doi:10.1029/2012WR012055, 2012.

760 Sivandran, G. and Bras, R.L.: Dynamic root distributions in ecohydrological modeling: A case study at Walnut Gulch Experimental Watershed, Water Resour. Res., 49(6), 3292-3305, doi:10.1002/wrcr.20245, 2013.

Smithwick, E.A.H., Lucash, M.S., McCormack, M.L. and Sivandran, G.: Improving the representation of roots in terrestrial models, Ecol. Model., 291, 193-204, doi:10.1016/j.ecolmodel.2014.07.023, 2014.

Shao, M., Wang, Y., Xia, Y. and Jia, X.: Soil drought and water carrying capacity for vegetation in the critical zone of the

765 loess plateau: a review, Vadose Zone J., 17(1), 170077, doi:10.2136/vzj2017.04.0077, 2018.

Shinozaki, K., Yoda, K., Hozumi, K. and Kira, T.: A QUANTITATIVE ANALYSIS OF PLANT FORM-THE PIPE MODEL THEORY: I.BASIC ANALYSES, Japanese Journal of Ecology, 14(3), 97-105, doi:10.18960/seitai.14.3_97, 1964.

Sun, L., Guan, W., Wang, Y., Xu, L. and Xiong, W.: Simulations of Larix principis-rupprechtii stand mean canopy stomatal conductance and its responses to environmental factors, Chin. J. Plant Ecol., 30(10), 2122-2128,

770 doi:10.3724/SP.J.1258.2011.00411, 2011(in Chinese with English abstract).

Thornton, P. E., Law, B. E., Gholz, H. L., Clark, K. L., Falge, E., and Ellsworth, D. S. et al.: Modeling and measuring the effects of disturbance history and climate on carbon and water budgets in evergreen needleleaf forests, Agric. For. Meteorol., 113(1-4), 185-222, doi:10.1016/S0168-1923(02)00108-9, 2002.

Tian, F., Feng, X., Zhang, L., Fu, B., Wang, S., Lv, Y., and Wang, P.: Effects of revegetation on soil moisture under

775 different precipitation gradients in the Loess Plateau, China, Hydrol. Res., 48(5), 1378-1390, doi:10.2166/nh.2016.022, 2017.

Tie, Q., Hu, H., Tian, F., Guan, H. and Lin, H.: Environmental and physiological controls on sap flow in a subhumid mountainous catchment in North China, Agric. For. Meteorol., 240, 46-57, doi:10.1016/j.agrformet.2017.03.018, 2017.

Trugman, A., Anderegg, L., Sperry, J., Wang, Y., Venturas, M., and Anderegg, W.: Leveraging plant hydraulics to yield

780 predictive and dynamic plant leaf allocation in vegetation models with climate change, Glob. Change Biol., 25(12): 4008-4021, doi:10.1111/gcb.14814, 2019.

Turkeltaub, T., Jia, X.X., Zhu, Y.J., Shao, M.A. and Binley, A.: Recharge and Nitrate Transport Through the Deep Vadose Zone of the Loess Plateau: A Regional-Scale Model Investigation, Water Resour. Res., 54(7), 4332-4346, doi:10.1029/2017WR022190, 2018.

785 Wang, J., Fu, B., Jiao, L., Lu, N., and Wang, L.: Age-related water use characteristics of *Robinia pseudoacacia* on the loess plateau, Agric. For. Meteorol., 301-302(5), 108344, doi:10.1016/j.agrformet.2021.108344, 2021.

Wang, P., Niu, G., Fang, Y., Wu, R., Yu, J., Yuan, G., Pozdniakov, S. P., and Scott, R. L.: Implementing Dynamic Root Optimization in Noah-MP for Simulating Phreatophytic Root Water Uptake, Water Resour. Res., 54(3), 1560-1575, doi:10.1002/2017WR021061, 2018a.

790 Wang, Y., Shao, M., Zhu, Y. and Liu, Z.: Impacts of land use and plant characteristics on dried soil layers in different climatic regions on the loess plateau of China, Agric. For. Meteorol., 151(4), 437-448, doi:10.1016/j.agrformet.2010.11.016, 2011.

Wang, Y., Shao, M., Zhu, Y., Sun, H. and Fang, L.: A new index to quantify dried soil layers in water-limited ecosystems: A case study on the Chinese Loess Plateau, Geoderma, 322, 1-11, doi:10.1016/j.geoderma.2018.02.007, 2018b.

795 Wang, Y., Shao, M., Liu, Z. and Zhang, C.: Characteristics of Dried Soil Layers Under Apple Orchards of Different Ages and Their Applications in Soil Water Managements on the Loess Plateau of China, Pedosphere, 25(4), 546-554, doi:10.1016/S1002-0160(15)30035-7, 2015.

Wang, Y., Xie, Z. and Jia, B.: Incorporation of a dynamic root distribution into CLM4.5: Evaluation of carbon and water fluxes over the Amazon, Adv. Atmos. Sci., 33(9), 1047-1060, doi:10.1007/s00376-016-5226-8, 2016.

800 Wang, Z., Liu, B., Liu, G. and Zhang, Y.: Soil water depletion depth by planted vegetation on the Loess Plateau, Science in China Series D-Earth Sciences, 52(6), 835-842, doi:10.1007/s11430-009-0087-y, 2009.

Warren, J. M., Hanson, P. J., Iversen, C. M., Kumar, J., Walker, A. P., and Wullschleger, S. D.: Root structural and functional dynamics in terrestrial biosphere models - evaluation and recommendations, New Phytol., 205(1), 59-78, doi:10.1111/nph.13034, 2015.

805 Wu, W., Li, H., Feng, H., Si, B., Chen, G., Meng, T., Li, Y. and Siddique, K.: Precipitation dominates the transpiration of both the economic forest (Malus pumila) and ecological forest (*Robinia pseudoacacia*) on the Loess Plateau after about 15

years of water depletion in deep soil, Agric. For. Meteorol., 297, 108244, doi:10.1016/j.agrformet.2020.108244, 2021.Xiao, Z., Liang, S. and Jiang, B.: Evaluation of four long time-series global leaf area index products, Agric. For. Meteorol., 246: 218-230, doi:10.1016/j.agrformet.2017.06.016, 2017.

810   Yang, W., Yan, B., and Huang D. et al.: MODIS leaf area index products: From validation to algorithm improvement, IEEE Geosci. Remote Sens. Lett., 44(7), 1885-1898, doi:10.1109/TGRS.2006.871215, 2006.

Yang, Y., Donohue, R. and McVicar, T.: Global estimation of effective plant rooting depth: Implications for hydrological modeling, Water Resour. Res., 52(10), 8260-8276, doi:10.1002/2016WR019392, 2016.

Zeng, X.: Global vegetation root distribution for land modeling, J. Hydrometeorol., 2(5), 525-530, doi:10.1175/1525-
815   7541(2001)002%3C0525:GVRDFL%3E2.0.CO;2, 2001.

Zhang, Y., Huang, M. and Lian, J.: Spatial distributions of optimal plant coverage for the dominant tree and shrub species along a precipitation gradient on the central Loess Plateau, Agric. For. Meteorol., 206, 69-84, 2015, doi: 10.1016/j.agrformet.2015.03.001, 2015.

Zhang, Z., Huang, M., Yang, Y. and Zhao, X.: Evaluating drought-induced mortality risk for *Robinia pseudoacacia*
820   plantations along the precipitation gradient on the Chinese Loess Plateau, Agric. For. Meteorol., 284, doi:10.1016/j.agrformet.2015.03.001, 2020.

Zhang, Z., Li, M., Si, B. and Feng, H.: Deep rooted apple trees decrease groundwater recharge in the highland region of the Loess Plateau, China. Sci. Total Environ., 622, 584-593, doi:10.1016/j.scitotenv.2017.11.230, 2018.

Zhao, C., Jia, X., Gongadze, K., Shao, M., Wu, L., & Zhu, Y.: Permanent dry soil layer a critical control on soil desiccation
825   on China's Loess Plateau, Sci. Rep., 9(1), 3296, doi:10.1038/s41598-019-38922-y, 2019.

Zhao, Y., Wang, Y., He, M., Tong, Y., Zhou, J., and Guo, X. et al.: Transference of *Robinia pseudoacacia* water-use patterns from deep to shallow soil layers during the transition period between the dry and rainy seasons in a water-limited region, Forest Ecol. Manag., 457, 117727, doi:10.1016/j.foreco.2019.117727, 2020.

Zuo, Q., Jie, F., Zhang, R. and Meng, L.: A generalized function of wheat's root length density distributions, Vadose Zone J.,
830   3(1), 271-277, doi:10.2136/vzj2004.2710, 2004.